FRONTIERS OF PHYSICS

RESEARCH ARTICLE
Volume 19 / Issue 4 / 42203 / 2024

Effect of ambient pressures on laser-induced breakdown spectroscopy signals

Kaifan Zhang[1], Weiran Song[1], Zongyu Hou[1,2], Zhe Wang[1,2,†]

1 State Key Laboratory of Power System Operation and Control, Tsinghua-Rio Tinto Joint Research Centre for Resources, Energy and Sustainable Development, International Joint Laboratory on Low Carbon Clean Energy Innovation, Institute for Carbon Neutrality, Department of Energy and Power Engineering, Tsinghua University, Beijing 100084, China

2 Shanxi Research Institute for Clean Energy, Tsinghua University, Taiyuan 030032, China

Corresponding author. E-mail: †zhewang@tsinghua.edu.cn

Received September 25, 2023; accepted December 24, 2023

ABSTRACT

Laser-induced breakdown spectroscopy (LIBS) is regarded as the future superstar for analytical chemistry and widely applied in various fields. Improving the quality of LIBS signal is fundamental to achieving accurate quantification and large-scale commercialization of LIBS. To propose control methods that improve LIBS signal quality, it is essential to have a comprehensive understanding of the influence of key parameters, such as ambient gas pressure, temperature, and sample temperature on LIBS signals. To date, extensive research has been carried out. However, different researchers often yield significantly different experimental results for LIBS, preventing the formation of consistent conclusions. This greatly prevents the understanding of influencing laws of key parameters and the improvement of LIBS quantitative performance. Taking ambient gas pressure as an example, this paper compares the effects of ambient gas pressure under different optimization conditions, reveals the influence of spatiotemporal window caused by inherent characteristics of LIBS signal sources, i.e., intense temporal changes and spatial non-uniformity of laser-induced plasmas, on the impact patterns of key parameters. From the perspective of plasma spatiotemporal evolution, the paper elucidates the influence patterns of ambient gas pressure on LIBS signals, clarifying seemingly contradictory research results in the literature.

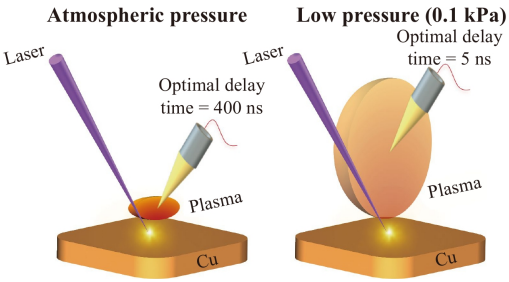

Keywords laser-induced breakdown spectroscopy, spatiotemporal window, pressure condition, signal uncertainty, plasma modulation

1 Introduction

Laser-induced breakdown spectroscopy (LIBS) is regarded as the future superstar for chemical analysis [1, 2]. Although it has a wide range of applications such as coal analysis [3], mineral processing and metallurgy [4], space exploration [5], and biological detection [6, 7], low spectral signal quality caused by fluctuated plasma remains a major bottleneck for the large-scale commercialization of LIBS. In the last decade, many methods have been developed to improve the spectral signal quality, including beam shaping [8], double-pulse configuration [9, 10], cylindrical confinement [11, 12], gas mixture and ambient pressure optimization [13, 14]. Furthermore, it

Higher Education Press

https://doi.org/10.1007/s11467-023-1380-5

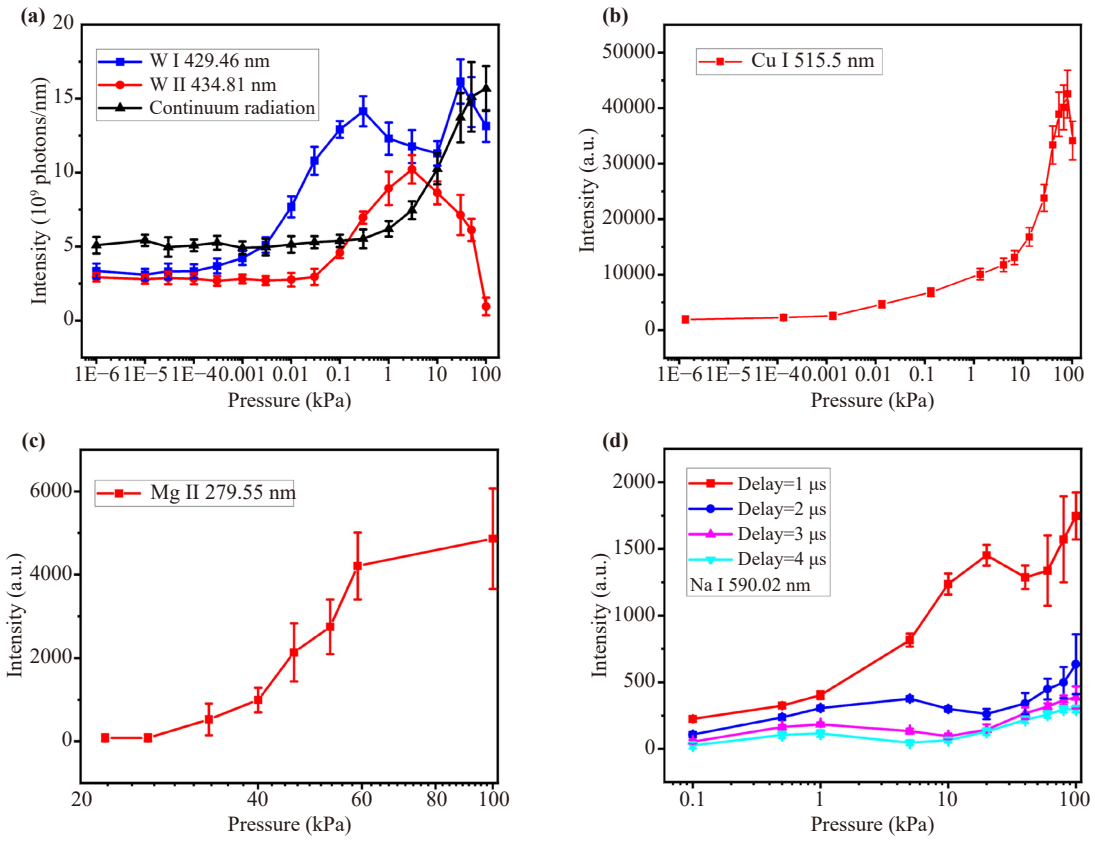

Fig. 1 Different results of pressure effects on the LIBS signal intensity from different researchers. **(a)** The absolute signal intensity of the continuum radiation, W II line (434.81 nm) and W I (429.46 nm) line as a function of air pressure [16]. **(b)** Variation in peak intensity of spectral line Cu I at 510.5 nm with pressure [18]. **(c)** Emission intensity of Mg II (279.55 nm) line at different pressures [19]. **(d)** Spectral intensity of Na I 590.02 nm under different air pressures [13].

is essential to have a comprehensive understanding of the influence of key parameters, such as ambient gas pressure, temperature, and sample temperature on LIBS signals to propose control methods that improve LIBS signal quality. Extensive research has been carried out but yield significantly different experimental results. In this paper, ambient gas pressure was chosen as an example for analysis, considering the intense and complex heat and mass transfer process between ambient gas and laser-induced plasma [15].

To investigate the ambient gas pressure effects on LIBS signals, the variation of spectral signal intensity at different pressures have been investigated. Wu *et al.* [16] produced laser-induced tungsten plasma at different pressures in air. As the pressure rises from 0.01 kPa to 3 kPa, the intensity of W II (434.81 nm) line increases to its maximum value, which is about four times the intensity at 0.01 kPa. When the pressure reaches 100 kPa, the intensity drops to about half of the intensity at 0.01 kPa, which is shown in Fig. 1(a). Farid *et al.* [17] studied the plasma parameters including spectral signal intensity, electron temperature and density at different environmental gases and pressures. Under air conditions, as the pressure increases from 0.67 kPa to atmospheric pressure, the Cu I (510.5 nm) line reaches its maximum intensity at 6.67 kPa and then decreases. Farid *et al.* [18] further investigated the influence of ambient pressure on the spectral signal intensity and expansion dynamics of a copper plasma plume. As shown in Fig. 1(b), the intensity of Cu I (510.5 nm) line attains its maximum value at 80 kPa, which is approximately 20 times higher than the signal intensity observed at 1.33×10^{-6} kPa. Haider *et al.* [19] conducted a comparison of the signal intensities between single-pulse and double-pulse laser ablation under different pressure conditions. Fig. 1(c) shows that the intensity of Mg II (279.55 nm) line monotonously increases with increasing pressure from 22 kPa to 100 kPa in the single-pulse configuration setting. Yi *et al.* [13] also obtained similar results in soil, with the intensity of Na I (590.02 nm) increasing with increasing pressure from 0.1 kPa to 100 kPa, as shown in Fig. 1(d). From above studies, the pressures corresponding to the maximal spectral signal intensities are different, even for the same spectral line of the same sample. Moreover, studies of plasma evolution at different pressures are limited in terms of observation time range [16, 18, 20]. These, together with the uncertainty of spectral signals [21], pose a challenge to study pressure

effects on LIBS signals and improvement on quantitative performance. Therefore, a comprehensive understanding of the plasma evolution process is needed to research pressure effects and improve signal quality.

Notably, the results due to pressure effect may vary because there are many variables that affect the spectral signals at different pressures, including sample characteristics, irradiance, gating delay and width and emission collection optics [22]. In fact, sample characteristics [17, 18] and irradiance [23] have relatively little effect on the spectral signals. Scott *et al.* [24] suggested that the optimal parameters of temporal window (delay time and gate width) are not fixed under different conditions. Wu *et al.* [16] showed that when the ambient gas pressure changes from 10^{-6} kPa to 10^{2} kPa, the optimal temporal window varies from 100 ns to 500 ns depending on the signal-to-background ratio and signal-to-background noise ratio. In addition, it is unclear how the spatial window (i.e., the spectral collection system position) affects the pattern of signal variation with pressure. The temporal and spatial windows are highly correlated and can be considered as spatiotemporal window. Currently, a fixed spatiotemporal window is commonly used when collecting spectra under different pressure conditions. However, the spatiotemporal evolution characteristics of the plasma undergo significant changes from low pressure to atmospheric pressure [25]. Moreover, the plasma region captured by the spectral collection system is only a small part of the whole plasma [26]. Thus, the position relative to the overall plasma and temporal evolution of this plasma region are distinct at different pressures. Furthermore, different series of the relative positions and temporal evolutions of the plasma region may be observed due to variations in experimental setups among different researchers. Therefore, different spatiotemporal windows may lead to different results in the literature.

In order to obtain a more comprehensive understanding of the phenomenon, it is recommended to optimize the spatiotemporal window for each pressure and capture a series of plasma evolution images when investigating the influence of ambient pressure on spectral signals. The collection of spectra with the optimal spatiotemporal window at each pressure can obtain the optimal spectral signal at that specific pressure. However, to the best of our knowledge, there is currently a lack of research on how the optimal spatiotemporal window for spectral collection varies with pressure. In this study, we validate that the variation in spatiotemporal windows for spectral collection can be one of the important factors leading to the different pressures where maximal spectral signal intensity occurs. The spatiotemporal window is optimized according to the best signal noise ratio (SNR) for each specific pressure. The reasons for the variation of the optimal spatiotemporal window are analyzed through plasma spatiotemporal evolution image. Spectral signals are collected using the optimal spatiotemporal window at each pressure to analyze the changes in spectral signal intensity and uncertainty with respect to pressure.

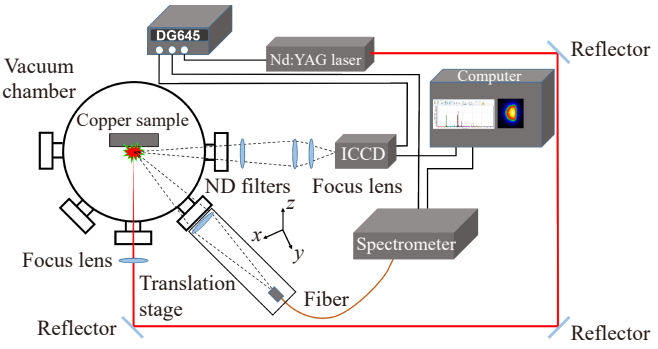

Fig. 2 Schematic diagram of the LIBS experimental setup. ND filters: neutral density filters.

Furthermore, we investigate the mechanisms behind the spectral signal intensity and uncertainty changes based on plasma spatiotemporal evolution image and ablated mass.

2 Experimental setup

The schematic diagram of the LIBS experimental setup in a vacuum chamber is shown in Fig. 2. A chamber is utilized in the experiment system which can be evacuated to a base pressure of 0.1 kPa by a pump, then the air was filled into the chamber through a reducing valve. A pulsed Nd:YAG laser (Dawa-200, Beamtech Optronics, China) with a wavelength of 1064 nm, a pulse duration of 7 ns, a laser energy of 100 mJ, and a repetition rate of 1 Hz was used for plasma generation. The laser beam was normally focused onto the target surface by an ultraviolet (UV) grade quartz lens with a 300-mm focal length. The laser power density was estimated to be 7.28 $\mathrm{GW{\cdot}cm^{-2}}$. A digital delay generator (DDG) was used to synchronize the laser, spectrometer, and intensified charge-coupled device (ICCD) camera (DH334T, Andor Technology Ltd, UK). The delay time of the spectrometer was optimized at each pressure, and the gate width was 1.05 millisecond as a default value determined by the instrument. The spectral collection system consists of a focal lens and an optical fiber, which are fixed on a translation stage. To achieve the 3-dimensional movement of the spectral collection system, the direction of 45° between the spectral collection system and the sample surface is used. The focus length and diameter of the collection lens is 125 mm and 25.4 mm, respectively. The diameter of the optical fiber of the spectrometer is 200 μm. Different spatial windows could be produced by moving the position of the translation stage. For each setting, 20 spectra were recorded at different positions. The evolution image of plasma was taken by ICCD camera and different integration times were set for different delay times to ensure the plasma images were clear. Integration times of 5 ns, 20 ns, 50 ns, and 100 ns were set for the plasma images taken between 5 ns to

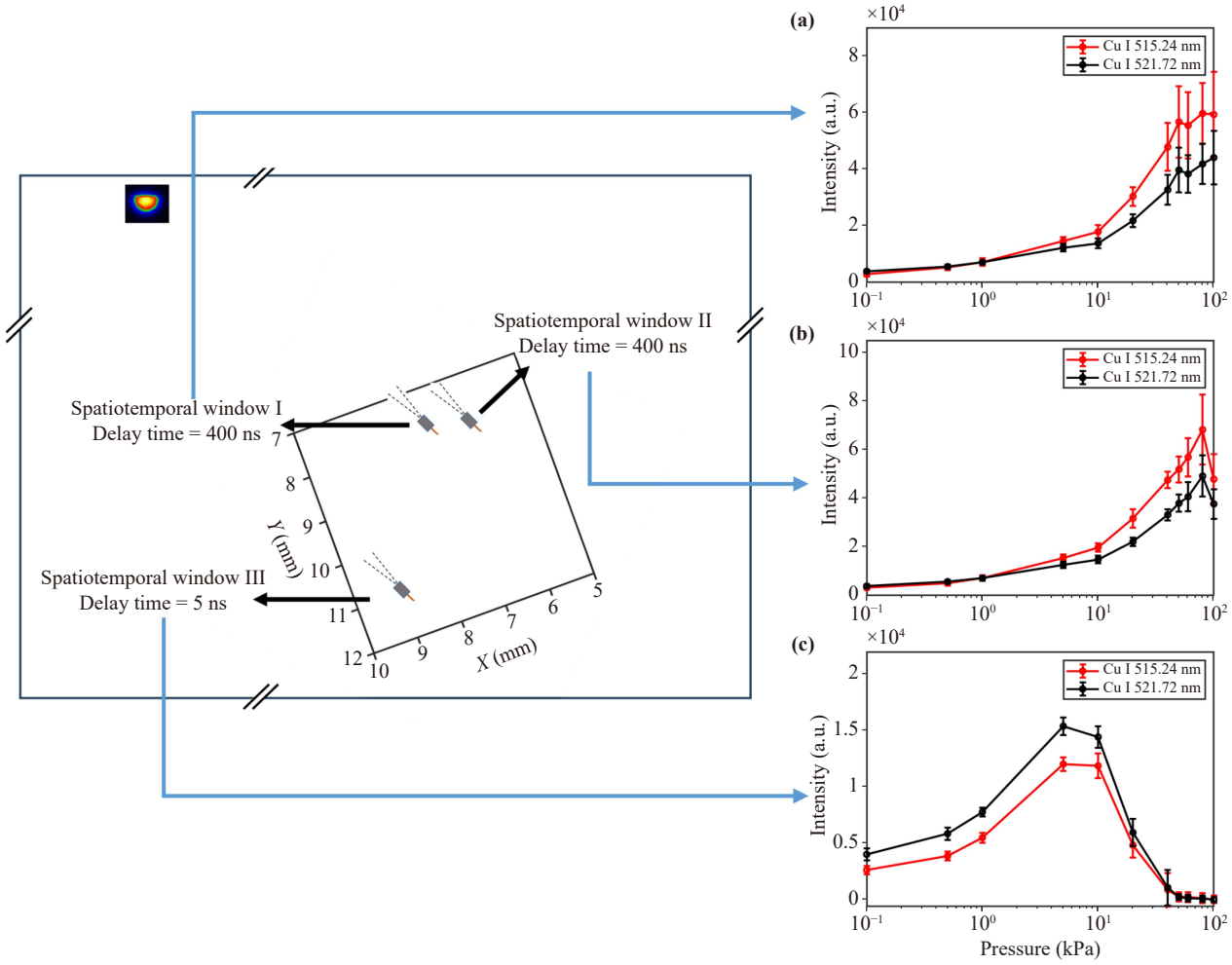

Fig. 3 The relative positions and delay time of spatiotemporal windows I, II, and III and patterns of LIBS signal intensity with pressure variation under spatiotemporal windows I **(a)**, II **(b)**, and III **(c)**. Omitted distances are denoted by // symbols for better visualization. X and Y are the coordinates of the translation stage in the horizontal plane direction.

250 ns, 300 ns to 700 ns, 1000 ns to 1700 ns, 2000 ns to 6000 ns, respectively. For each delay time, 20 pulses were applied at different positions on the sample surface to obtain the plasma images. The ablation crater was measured by using a confocal microscope at a magnification of 20. A pure copper (Cu > 99.9%) target was used in this study and was mounted on a translation stage. Pure copper was polished by sand paper and then rinsed by alcohol.

3 Results and discussion

3.1 The influence of the spatiotemporal window on the pattern of LIBS signal intensity with pressure

As discussed in the introduction, the spatiotemporal window plays a crucial role in determining the pattern of spectral signal intensity variation with pressure. Different patterns in the variation of spectral signals with pressure can be obtained when varying the spatiotemporal window according to previous analysis. By changing the delay time of the spectrometer and the position of the spectral collection system, we generated different spatiotemporal windows and observed the patterns of spectral signal intensity variation with pressure under these spatiotemporal windows.

Figure 3(a) illustrates the spectral signal intensity of Cu I (515.24 nm) and Cu I (521.72 nm) lines variation under spatiotemporal window I optimized at 100 kPa with pressure variation. The signal intensity increases with an increase in pressure from 0.1 kPa to 100 kPa, which agrees with the results reported in Ref. [19]. Figure 3(b) demonstrates the spectral signal intensity variation of Cu I (515.24 nm) and Cu I (521.72 nm) line under spatiotemporal window II optimized at 80 kPa with pressure variation. As the pressure increases from 0.1 kPa to 100 kPa, the signal intensity initially increases, attains its maximum at 80 kPa, which is consistent with the results reported in reference [18]. Figure 3(c) illustrates the spectral signal intensity variation of Cu I

(515.24 nm) and Cu I (521.72 nm) line under spatiotemporal window III optimized at 5 kPa with pressure variation. As the pressure increases from 0.1 kPa to 100 kPa, the signal intensity increases initially, reaches its maximum at 5 kPa, and then decreases, which is almost consistent with the results reported in Refs. [16, 17, 27].

Coaxial to laser axis optical configuration, perpendicular to laser axis optical configuration, sloping to laser axis optical configuration was used in Ref. [16], Refs. [17, 18, 27], and Ref. [19], respectively. It is challenging to analyze the reasons for different results based on the literature's spectra collection systems. The results of the pattern of spectral signal intensity with pressure vary even with the same type of spectra collection system [17, 18]. The variability in specific configurations, such as the focal length and position of the lens, exists even among spectral collection systems of the same type. Coupled with differences in the instrumentation and settings, it is difficult to ascertain the underlying reason for the different results. Accordingly, the delay time of the spectrometer and the position of the spectral collection system were adjusted to modify the spatiotemporal windows in this study. This allowed for a clear investigation of the influence of the spatiotemporal window. Figure 3 displays the relative positions and delay time of spatiotemporal windows I, II, and III. The distribution of the grey rectangles in the axes represents the relative positions of the optical fiber.

Compared to spatiotemporal windows I and II, spatiotemporal window III is more distant from the sample surface and earlier in delay time. This corresponds to the larger expansion region and a quicker decay of the plasma at 5 kPa. Under spatiotemporal window III, the spectral signals emitted during the initial stage of plasma evolution at approximately 5 kPa can be captured, while it is unable to capture the spectral signals of the plasma at 100 kPa due to the limit of spatiotemporal window and the small plasma expansion region of 100 kPa. Therefore, the corresponding results show stronger spectral signals at 5 kPa. For spatiotemporal windows I and II, they are closer to the sample surface, and the delay time is relatively later. This is consistent with the observation that the plasma expands in a confined region and decays more slowly at around 100 kPa. Consequently, for these two spatiotemporal windows, the spectrometer primarily captures the spectral signals corresponding to the plasma region at around 100 kPa. However, it can only capture little spectral signals from the plasma region at pressures below 5 kPa due to the limited plasma life and the large plasma expansion region. As a result, the spectral signal intensity is relatively stronger at 100 kPa and weaker at 5 kPa. Spatiotemporal window I is closer to the sample surface than spatiotemporal window II. As a result, spatiotemporal window I is able to capture more spectral signals from the plasma at 100 kPa, leading to stronger spectral signals at 100 kPa.

3.2 Variation of optimal spatiotemporal windows at each pressure and mechanism analysis

As stated in Section 3.1, the spatiotemporal window plays a critical role in investigating the influence of pressure on spectral signals. The diameter of the collection region corresponding to the fiber is estimated to be 181.16 μm in the direction perpendicular to the optical axis of the spectral collection system. The size is relatively small compared to the plasma size especially under the low-pressure condition [26]. Thus, the spatiotemporal window for spectral collection is optimized at each pressure by taking into account the significant changes in plasma evolution. Due to the strong correlation between the time window and spatial window, the optimal spatial window corresponding to different temporal windows may vary, and vice versa. Therefore, the optimization of the spatiotemporal window is an iterative process. Figure 4(a) shows the details of the iterative process of optimizing the spatiotemporal windows at each pressure. When starting with a pressure of 100 kPa, the initial delay time d_1 is set to 5 ns for optimizing the optimal spatial window based on the best signal-to-noise ratio (SNR). The SNR could be calculated as

$$SNR = \frac{I}{\sigma}, \tag{1}$$

where I is the intensity of Cu I (521.72 nm) line, and σ is the standard deviation of the continuum background within a 3 nm region of the spectrum where there is no obvious line emission. After obtaining the optimized spatial window (position i), the delay time is further optimized, resulting in a new delay time d_{i+1}. The equivalence between d_{i+1} and time d_i is checked, and if they are not equal, i is updated to be equal to $i+1$. This iterative process is repeated until d_{i+1} is equal to d_i, at which point the delay time and spatial window correspond to the optimal spatiotemporal window. For the next pressure, the initial delay time will be set to the optimal delay time obtained from the previous pressure for efficient adjustment of the spatiotemporal window at the new pressure. Figure 4(b) shows the optimal spatial and temporal windows at different pressures, which will be discussed in the following sections in details.

In order to gain a comprehensive understanding of the spatiotemporal evolution of the plasma at different pressures, we captured plasma images at each pressure with delay times ranging from 5 ns to 6000 ns at each pressure, Fig. 5 shows the plasma evolution images at specific pressures and delay times. Each image is averaged by 20 plasma images and normalized according to the maximum value and minimum value of plasma image intensity. From Fig. 5, the plasma expands only within a limited area at 100 kPa. However, as the pressure decreases, the plasma expansion area gradually increases; when the pressure decreases to 0.1 kPa, the plasma expansion range is significantly larger, reaching

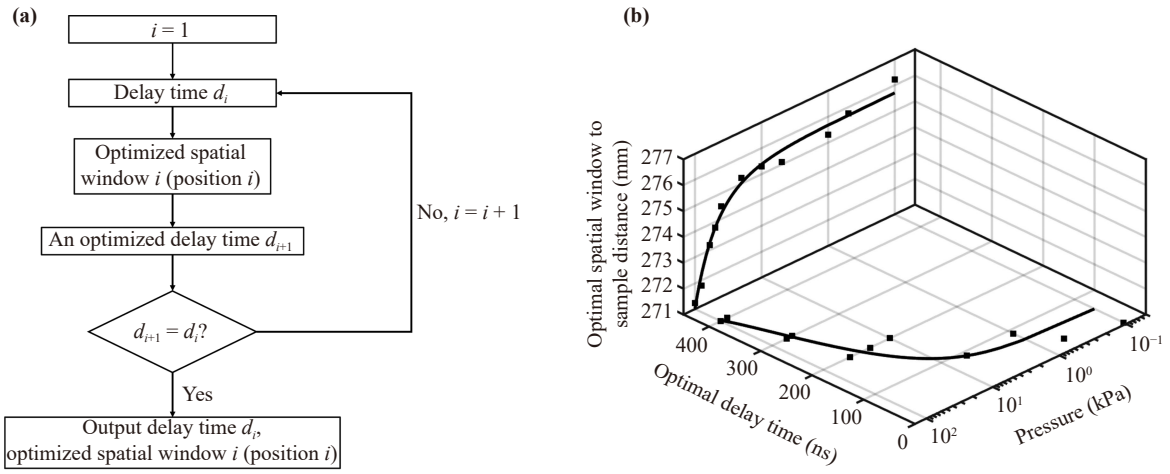

Fig. 4 **(a)** The iterative process of optimizing the spatiotemporal windows at each pressure. **(b)** The optimal spatial and temporal windows at different pressures. The black cubes represent the experimental results, while the curve represent the fitted values based on the results.

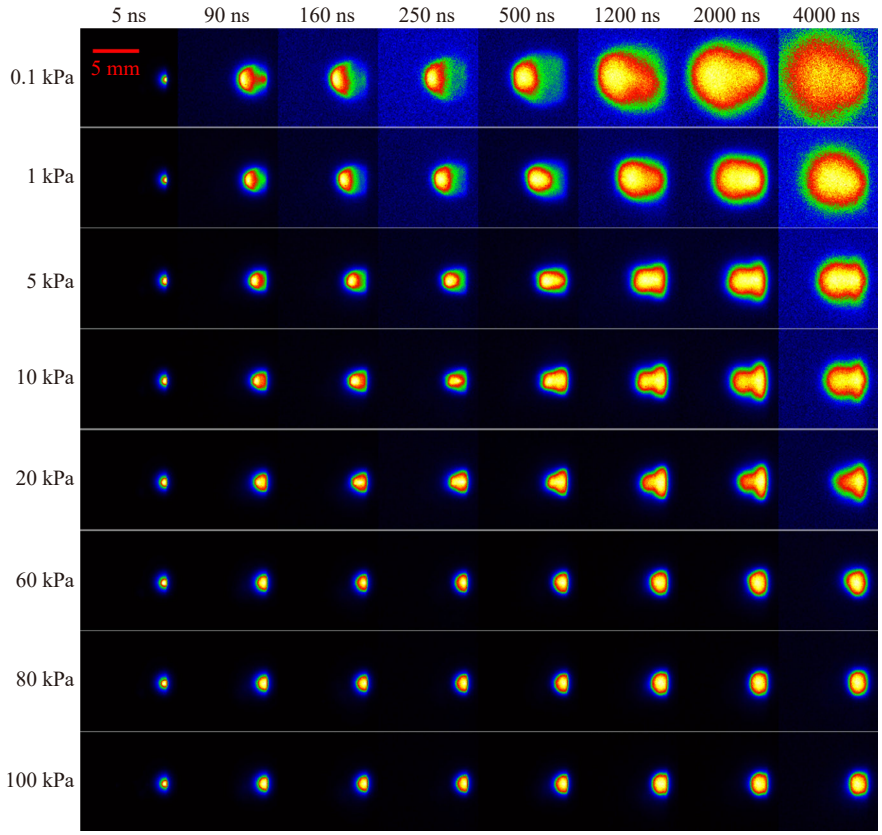

Fig. 5 The plasma evolution images at different pressures.

nearly 11 mm. The detailed discussion of the plasma's time evolution at different pressures will be presented in Section 3.2.1.

3.2.1 Optimal temporal windows at each pressure and mechanism analysis

As shown in Fig. 4(b), the optimal temporal window varies with pressure. According to the iterative process of optimization of the spatiotemporal window, the optimal temporal window can be identified by the delay time corresponding to the best signal-to-noise ratio (SNR) during the final iteration, which is shown in Fig. 6(a) partly. The SNR values are normalized by dividing the maximum value at each pressure. At the pressure of 100 kPa, the SNR gradually increases with an extension

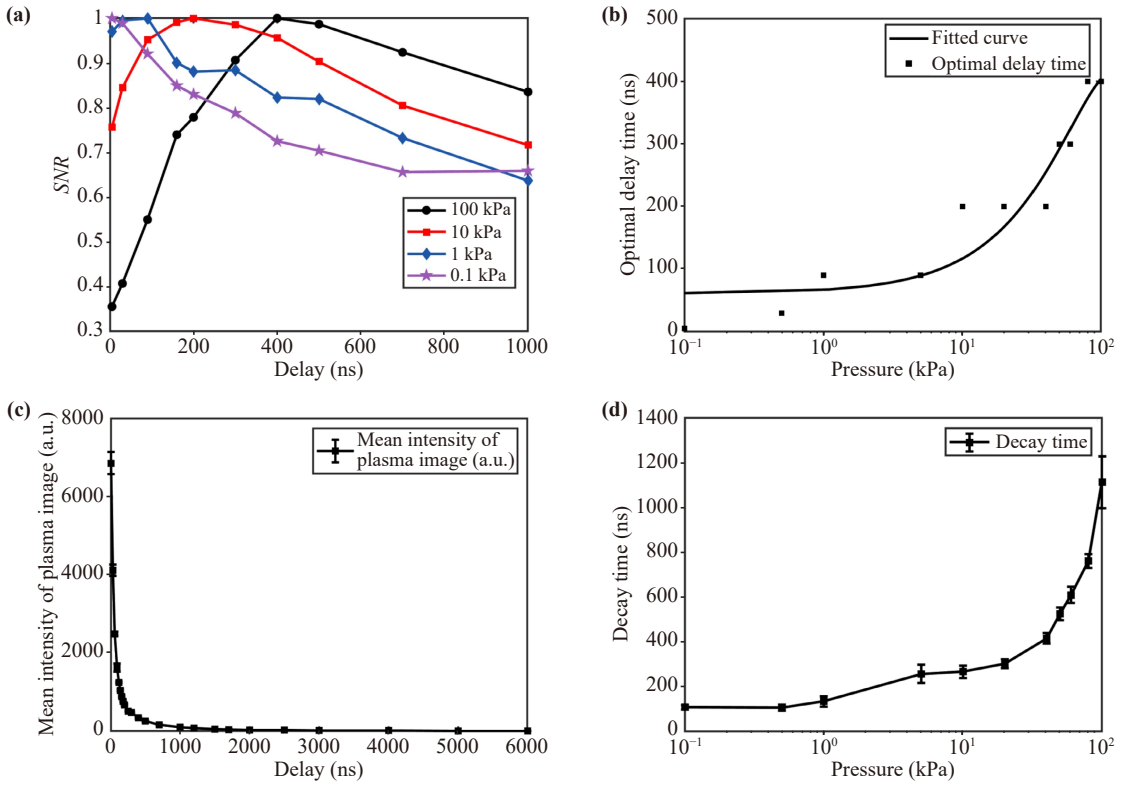

Fig. 6 **(a)** The variation of signal-to-noise ratio (*SNR*) of Cu I (521.72 nm) line with delay during the final iteration of spatiotemporal window optimization. **(b)** The optimal delay time at different pressures. The black squares represent the experimental results, while the curve represent the fitted values based on the results. **(c)** The variation of average plasma image intensity over time at 100 kPa. **(d)** The variation of plasma decay time with pressure.

of delay time, reaching a maximum at 400 ns, and thereafter gradually decreases. The maximum values of the SNR occur at 200 ns and 90 ns for lower pressures such as 10 kPa and 1 kPa, respectively. When the pressure is 0.1 kPa, the SNR decreases with delay time from 5 ns. The best signal-to-noise ratio of the spectral signals at different pressures occurs at different delay times, therefore different pressures correspond to different optimal temporal windows. Figure 6(b) shows that the optimal delay time shifts to later delays progressively, from 5 ns to 400 ns, as pressure increases from 0.1 kPa to 100 kPa.

Spectral signal background change and plasma decay are responsible for different optimal temporal windows at different pressures. Scott *et al.* [24] found that the spectral signal background is much lower at low pressures than at the atmospheric pressure. As the pressure decreases from atmospheric pressure, the continuum radiation decreases monotonically up to about 0.1 kPa, then remains almost constant [16]. As the spectral signal intensity decreases with delay time, the decline of background can cause the optimal temporal window to occur at an early delay time. Further analysis of the plasma images shows that the decrease in the spectral signal background with decreasing pressure is due to a faster decay of the plasma. The plasma boundary was defined as $1/e$ of the maximum intensity of each plasma image, and the average intensity of the plasma was calculated. The plasma decay time is defined as the time required for the average intensity of the plasma image to decrease to 5% of the average intensity at 5 ns, representing relative values of plasma lifetime. Figure 6(c) shows the variation of the average plasma image intensity over time at 100 kPa. During the initial 1000 ns, the average plasma intensity decreases rapidly. Subsequently, it gradually decreases at a slow rate.

The variation of the plasma decay time with pressure is shown in Fig. 6(d). The decay time increases with increasing pressure. The plasma decay time at 100 kPa is about 10 times longer than at 0.1 kPa. This indicates that the plasma has a longer lifetime at atmospheric pressure. As the pressure increases, the stronger confinement can lead to larger plasma decay time and longer lifetime. At 100 kPa, as the plasma decays more slowly, the spectral signal background noise decays slower as well, resulting in the high background noise existing for a relatively longer period of time, causing the optimal time window for spectral collection to have to be shifted backward. At low pressures, the plasma decays very rapidly and the background noise of spectral signal also decreases very rapidly, resulting in the high spectral signal background noise being present for only a relatively short period of time. Therefore, the optimal time

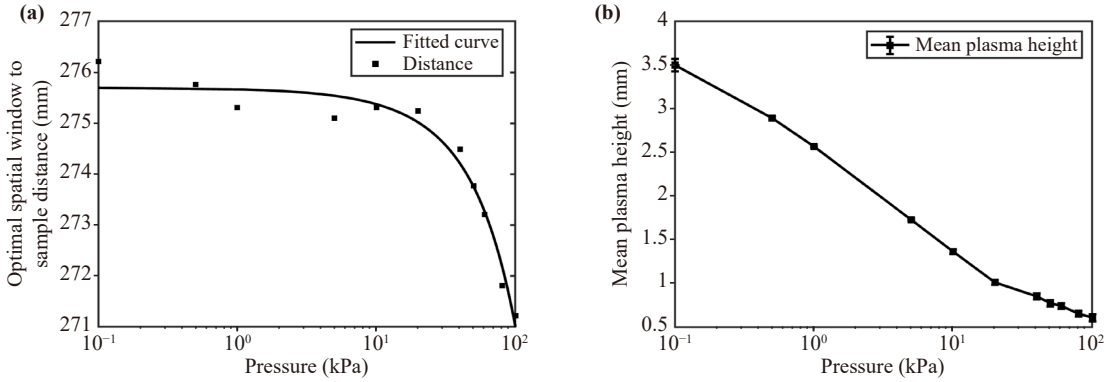

Fig. 7 **(a)** The variation of the optimized window to sample distance with respect to pressure. **(b)** The variation of the mean plasma height with respect to pressure.

windows for spectral collection can be earlier at low pressures.

3.2.2 Optimal spatial windows at each pressure and mechanism analysis

The variation of optimal spatial window-to-sample distance with respect to pressure is shown in Fig. 7(a). The distance of the optimal spatial window to the sample is calculated from the coordinates of the x–y–z stage. As the pressure increases, the optimal spatial window gradually approaches the sample surface. The distance of the spatial window to the sample varies from 276.21 mm to 271.22 mm, as the pressure increases from 0.1 kPa to 100 kPa. At the range of 0.1–10 kPa, this change is not very significant; at the range of 10–100 kPa, the position of the spatial window moves towards the sample more quickly. The variation of the optimal spatial window at some pressures (e.g., 5 kPa and 10 kPa) does not exactly fit this pattern, which is due to the variation of their delay times. The spatial window of 10 kPa and 5 kPa corresponds to a delay time of 200 ns and 90 ns, respectively. The advancement of the delay time at 5 kPa leads to the optimal spatial window closer to the sample. This phenomenon demonstrates the coupling effect of temporal and spatial windows.

The position of the optimal spatial window is related to the expansion characteristics of the plasma. To clarify the reason for the variation in the optimal spatial window, the average height (relative to the sample) of gravity center of plasma for 24 delay times was calculated, as shown in Fig. 7(b). As the pressure increases, the main region of plasma expansion moves closer to the surface of the sample surface. The average plasma height decreases from 3.5 mm to 0.61 mm as pressure changes from 0.1 kPa to 100 kPa, which is consistent with the changes in the optimal spatial window position with pressure.

3.3 Pressure effect on spectral signal intensity and uncertainty

From Section 3.2, it is clear that there are significant differences in the optimal spatiotemporal windows and the plasma evolution process under different pressures. Therefore, this paper uses the optimal spatiotemporal windows at each pressure to investigate the patterns of signal intensity and uncertainty. By analyzing the plasma images and ablation crater volumes, this study investigates the mechanism behind the changes in spectral signal intensity and uncertainty with respect to pressure.

3.3.1 Pressure effect on the spectral signal intensity, SNR and SBR

Within the optimal spatiotemporal window at each pressure, the plasma spectral signal intensity was collected by the spectrometer. As shown in Fig. 8(a), the spectral signal intensity of Cu I (515.24 nm) and Cu I (521.72 nm) lines increases with increasing pressure in the range of 0.1 kPa to 60 kPa, and then decreases with further increase in pressure from 60 kPa to 100 kPa. Compared to the results in Section 3.1, the intensity of the spectral signal at 60 kPa is stronger under the optimal spatiotemporal window of 60 kPa. This suggests that a fixed spatiotemporal window is not appropriate for evaluating the spectral signal intensity at different pressures. To investigate the mechanism of the variation of spectral signal intensity with pressure, the plasma images and the sample ablation volume were analyzed.

In this study, the average area of the plasma images at different pressures was calculated, as shown in Fig. 8(b). As the pressure increases from 0.1 kPa to 100 kPa, the average area of the plasma decreases monotonically, indicating a reduction in the plasma volume. The decrease in the plasma volume results in an increase in the number density of particles within a confined space, leading to an enhanced spectral signal intensity. However, when the particle number density is sufficiently

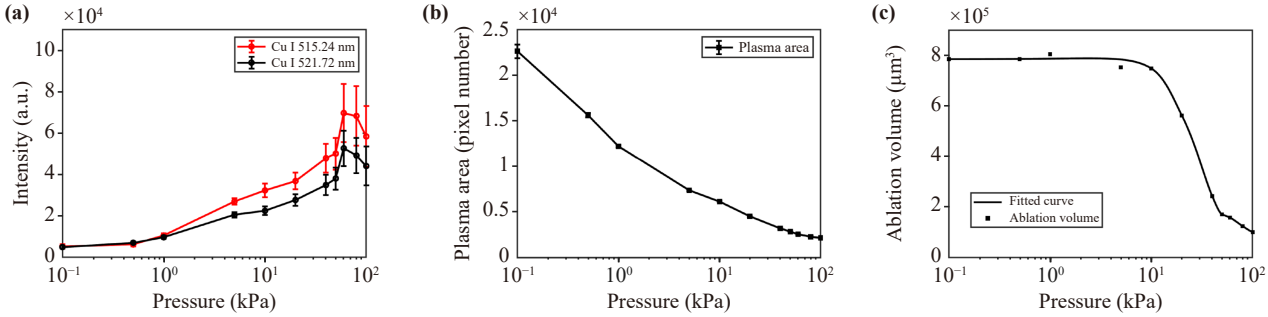

Fig. 8 **(a)** The patterns of spectral signal intensity of Cu I (515.24 nm) and Cu I (521.72 nm) lines with respect to pressure under the optimal spatiotemporal windows at each pressure. **(b)** Variation of the plasma area with pressure. **(c)** The variation of the accumulated volume of laser ablation craters with pressure after 50 laser pulses.

high, the plasma shielding effect occurs, leading to a reduction of the sample ablation mass. In this study, the volume of ablation craters obtained by confocal microscopy was used to represent the ablation mass.

Figure 8(c) shows the variation of the accumulated volume of laser ablation craters with pressure after 50 laser pulses. In the vicinity of 0.1 kPa to 10 kPa, the volume of the ablation craters remains relatively constant. From 10 kPa to 100 kPa, the volume of the craters decreases rapidly, similar to the results reported in the literature [16]. This suggests that the pattern of ablation mass with pressure is characterized by a relatively constant mass in the range of 0.1 kPa to 10 kPa, followed by a rapid decrease in mass from 10 kPa to 100 kPa. Figure 9 shows the 3D images of ablation craters at 0.1 kPa and 100 kPa. The top image corresponds to the case at 0.1 kPa, while the bottom image corresponds to the case at 100 kPa. On the left side of Fig. 9, the depth profile of the ablation crater in the center section is shown. At 0.1 kPa, the maximum depth of the ablation crater reaches 25.04 mm and is uniformly distributed in the Y direction. At 100 kPa, the maximum depth of the ablation crater was only 5.66 mm and was not uniformly distributed in the Y direction. On the right side, the 3D representation of the ablation crater image is displayed. At 0.1 kPa, a relatively deep area is clearly visible in the ablation crater image. At 100 kPa, the morphology of the ablation pit is not very regular. The small amount of ablation at atmospheric pressure, combined with the presence of some roughness on the sample surface, leads to the irregularity at 100 kPa. At 0.1 kPa, the ablation crater exhibits a significantly larger volume and greater depth compared to that at 100 kPa. Compared to the low pressure conditions, the ablation mass is lower at atmospheric pressure, which is also reported in other references [18, 24, 28].

As the pressure increases from 0.1 kPa, the confinement effect of the ambient gas on the plasma intensifies. Consequently, the plasma volume decreases while the particle number density increases, leading to an enhancement in the spectral signal intensity. As the pressure increases to around 10 kPa, the shielding effect on the plasma occurs, resulting in a decrease in plasma ablation. The spectral signal intensity enhancement due to the decrease in plasma volume and the spectral signal intensity reduction due to the decrease in plasma ablation occur simultaneously. At 10–60 kPa, the spectral signal intensity enhancement due to the decrease in plasma volume dominates and the spectral signal intensity enhances. At 60 kPa to 100 kPa, the spectral signal intensity reduction due to the decrease in plasma ablation volume dominates and the spectral signal intensity decreases.

Figure 10 shows signal-to-noise and signal-to-background of Cu I (515.24 nm) and Cu I (521.72 nm) lines under the optimal spatiotemporal window at each pressure. The signal-to-background (SBR) could be calculated with formula (2), where I is the intensity of spectral line, and I_B is the average value of the continuum background within a 3 nm region of the spectrum where there is no obvious line emission. It is important to note that the obtained continuum background and background noise are also under the optimal spatial and temporal window at each pressure. It can be seen from Fig. 10(a) that the trend of SNR with pressure is consistent with the trend of signal intensity with pressure. This is due to the relatively small change in background noise at different pressures. Figure 10(b) shows that the SBR increases and then decreases with the enhancement of pressure, reaching a maximum at 1 kPa. This is due to the fact that the absolute value of the continuum background decreases with decreasing pressure,

$$SBR = \frac{I}{I_B}. \tag{2}$$

3.3.2 Pressure effect on the spectral signal uncertainty

Within the optimal spatiotemporal window at each pressure, the plasma spectral signal uncertainty is represented by the relative standard deviation (RSD) of spectral

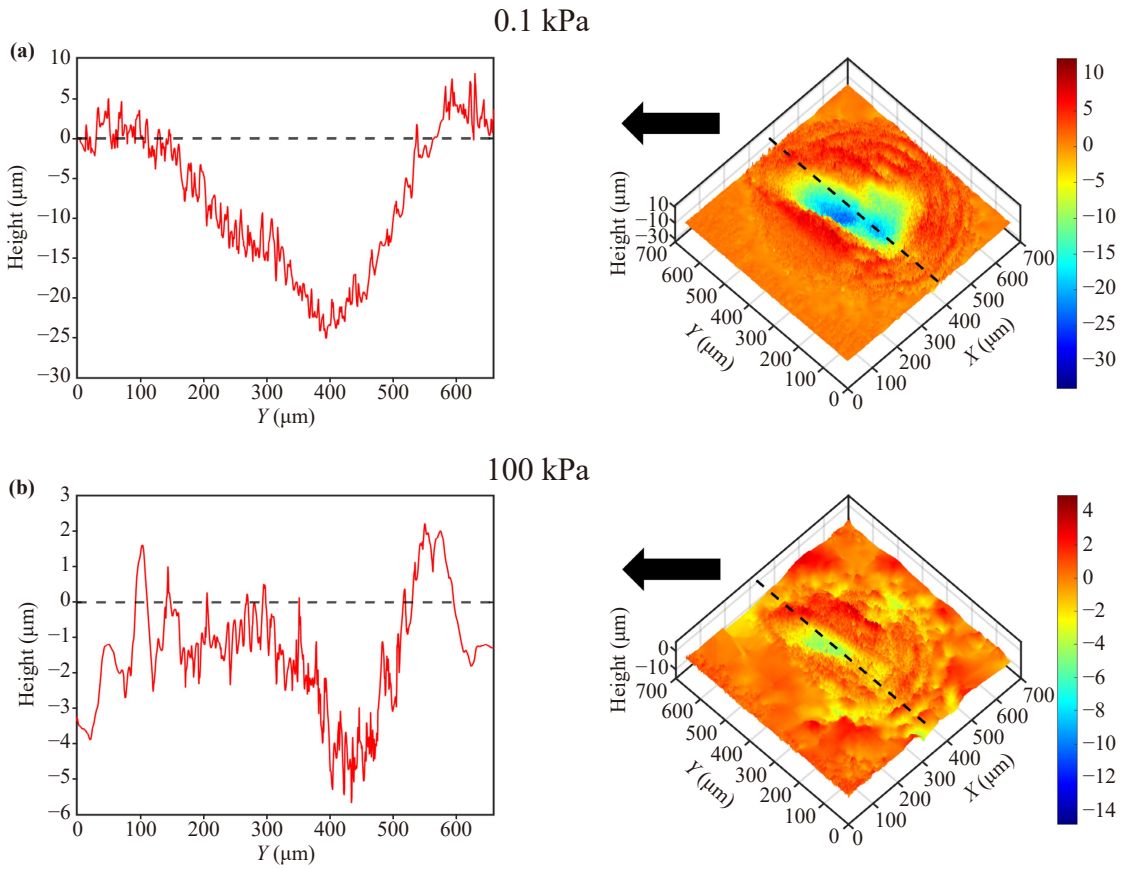

Fig. 9 The depth and 3D images of ablation craters at 0.1 kPa **(a)** and 100 kPa **(b)**.

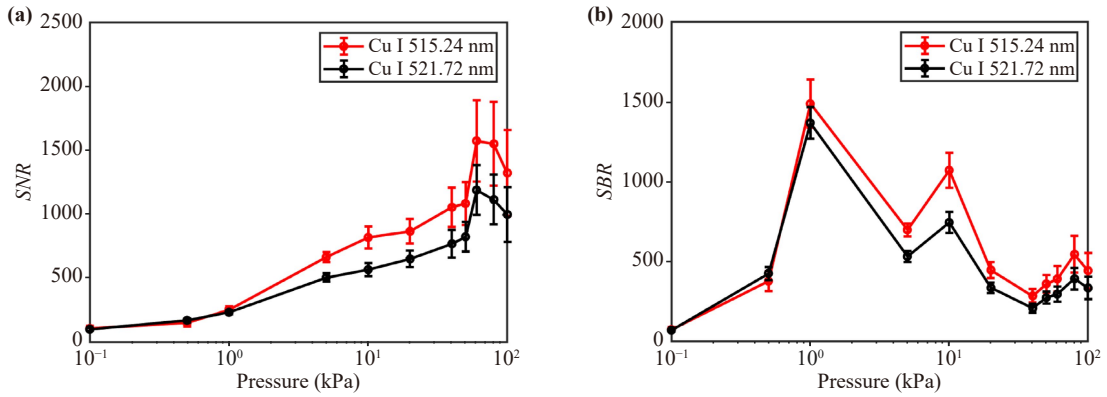

Fig. 10 Signal-to-noise **(a)** and signal-to-background **(b)** of Cu I (515.24 nm) and Cu I (521.72 nm) lines at different pressures.

signal intensity. As shown in Fig. 11, the RSD of Cu I (515.24 nm) and Cu I (521.72 nm) line intensities decrease with increasing pressure in the range of 0.1 kPa to 5 kPa, and then increases from 5 kPa to 100 kPa. The RSD of the Cu I (521.72 nm) line can be as low as 5.89% at 5 kPa.

The key process leading to the spectral signal uncertainty is studied by Fu *et al.* [15]. The morphology fluctuation of the plasma is a contributing factor. As shown in Fig. 12, the results indicate that the morphology of the plasma remains stable up to 100 ns, after which it starts to fluctuate more and more until it becomes into a "fluctuating plasma" after 270 ns. During this period, there is a back-pressing process in the frontier part of the plasma due to the pressure gradient directed to the sample surface. Due to the force produced by pressure gradient in the plasma pointing toward the sample surface, a rebound phenomenon occurs at the plasma front. The rebounding frontier species collide with the lower plasma, resulting in horizontal expansion of the plasma

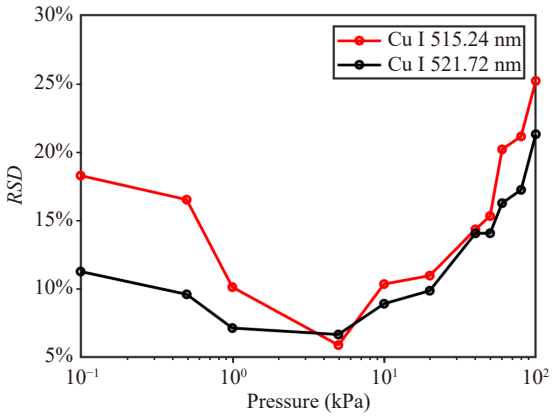

Fig. 11 The spectral signal intensity *RSD* with respect to pressure under the optimal spatiotemporal windows at each pressure.

and causing instability of the plasma morphology.

To summarize, the back-pressing and crash processes can greatly affect the morphological stability of the plasma, which in turn affects the spectral signal uncertainty. In order to study the back-pressing and collision processes of the plasma, an ICCD was used to capture time-evolving images of the plasma at different pressures. Figure 13 shows the plasma evolution images over time at 0.1 kPa, 5 kPa, and 100 kPa. Each image is normalized according to the maximum and minimum values of plasma image intensity. At 0.1 kPa, the plasma shows a weak rebound phenomenon starting at about 1700 ns and lasting until 4000 ns. Early in the plasma evolution (at 60 ns and 90 ns), the plasma appears to segregate, which is consistent with results in the literature [18, 20]. The plasma then expands outwards until 1700 ns. At 2000 ns, an increase in the intensity of the plasma plume back appears, indicating that the front of the plasma is rebounding backward. This process continues until about 4000 ns. The plasma then gradually expands outwards again, forming an almost circular shape. At 5 kPa, the plasma starts to rebound around 700 ns and continues until 2000 ns, followed by further expansion. Early in the plasma evolution, the plasma expands outwards rapidly. By 700 ns, the plasma expansion is hindered and begins to bounce back towards the sample surface, causing the plasma to expand perpendicular to the laser direction in the region near the sample. This process continues until about 2000 ns, after which the plasma gradually expands outwards again, forming an almost elliptical shape. At 100 kPa, the plasma starts to rebound around 120 ns and continues until 180 ns, followed by further expansion. At this pressure, the plasma expands up to 120 ns and then rebounds, causing the plasma to create an expansion perpendicular to the laser direction. At the end of the rebound process, the plasma expands outwards again, eventually forming an ellipse.

Figure 14 shows more clearly the movement of the core region of the plasma from 5 ns to 6000 ns. In each plasma image, the top 10% brightness region is considered to be the core region of the plasma. The unit of coordinates is the number of pixels, and the vertical axis in Fig. 14 represents the distance of the center of gravity of the plasma core region from the sample surface. It can be clearly seen that the plasma rebound process occurs in the time ranges of 1700–4000 ns, 700–2000 ns, and 120–180 ns at 0.1 kPa, 5 kPa, and 100 kPa, respectively.

As the pressure decreases, the occurrence of the plasma rebound process is progressively delayed. The longer time that the plasma is in stable morphology, coupled with the stronger spectral signal early in the plasma's life, results in the spectral signal containing a greater proportion of the stable signal. Therefore, the RSD of the spectral signal gradually decreases as the pressure decreases. However, as the pressure decreases

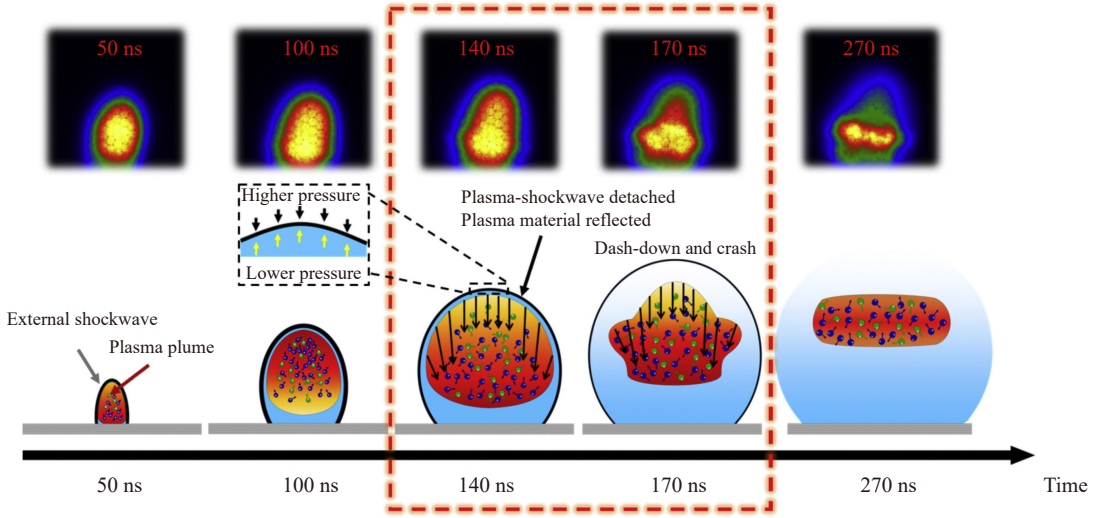

Fig. 12 The diagram of plasma and external shock wave evolution [15].

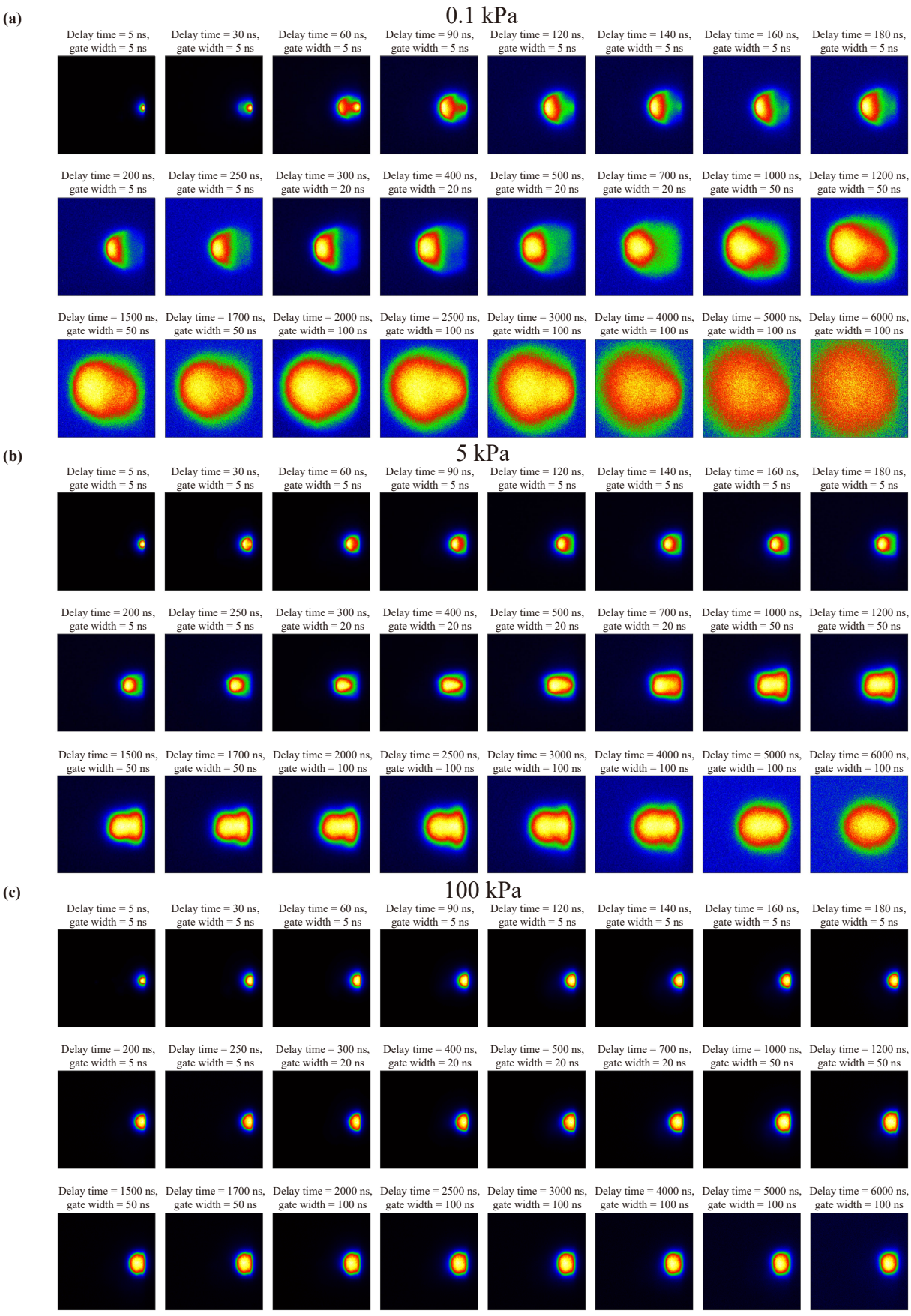

Fig. 13 Plasma evolution images over time at 0.1 kPa **(a)**, 5 kPa **(b)**, and 100 kPa **(c)**.

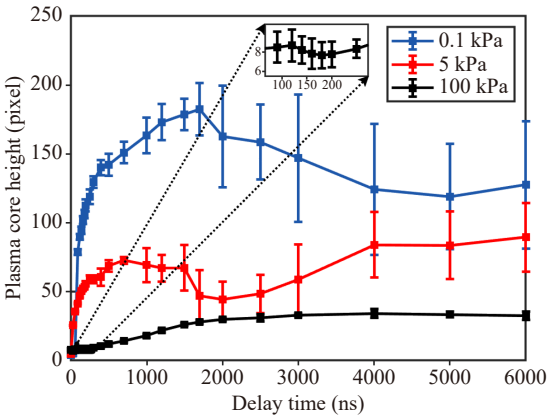

Fig. 14 The variation of the plasma core region height with delay time at pressures of 0.1 kPa, 5 kPa, and 100 kPa.

from 5 kPa to 0.1 kPa, although the plasma rebound process is further delayed, the significant decrease in signal intensity due to plasma expansion leads to an increase in RSD. To summarize, 5 kPa is the best pressure to obtain the lowest RSD for the pure copper sample.

4 Conclusion

This paper validates the significant role of the spatiotemporal window in collecting LIBS signals at different pressures. Different spatiotemporal windows can lead to different patterns of LIBS signal changes with pressure, which may be one of the reasons for the different results in the literature. The optimal spatiotemporal window varies significantly at different pressures: as the pressure changes from 0.1 kPa to 100 kPa, the optimal temporal window increases from 5 ns to 400 ns, which is attributed to the increase in plasma lifetime with increasing pressure. The optimal spatial window changes by 4.99 mm, which is due to the significant reduction in the expanding region of the plasma with increasing pressure. At each pressure, the optimal spatiotemporal window was used to collect the spectral signals. The changes in signal intensity and RSD at different pressures were calculated and analyzed. The signal intensity increased from 0.1 kPa to 60 kPa and then decreased from 60 kPa to 100 kPa. This pattern is a result of the combined effects of ablation mass and plasma expansion variations. On the other hand, the RSD decreased from 0.1 kPa to 5 kPa and then increased from 5 kPa to 100 kPa. This phenomenon is attributed to the enhancement of the spectral signal and the progressively earlier occurrence of the plasma rebound process with increasing pressure. In future research on factors influencing LIBS signal, we recommend to consider the influence of the spatiotemporal window on the spectral signal and focus on the changes in the complete spatiotemporal evolution of the plasma in order to obtain a comprehensive understanding.

Declarations The authors declare that they have no competing interests and there are no conflicts.

Acknowledgements The authors are grateful for the financial supports from the National Key Research and Development Program of China (No. 2023YFB4102900).

References

1. Z. Wang, T. B. Yuan, Z. Y. Hou, W. D. Zhou, J. D. Lu, H. B. Ding, and X. Y. Zeng, Laser-induced breakdown spectroscopy in China, *Front. Phys.* 9(4), 419 (2014)
2. J. D. Winefordner, I. B. Gornushkin, T. Correll, E. Gibb, B. W. Smith, and N. Omenetto, Comparing several atomic spectrometric methods to the super stars: Special emphasis on laser-induced breakdown spectrometry, LIBS, a future super star, *J. Anal. At. Spectrom.* 19(9), 1061 (2004)
3. S. Sheta, M. S. Afgan, Z. Hou, S. C. Yao, L. Zhang, Z. Li, and Z. Wang, Coal analysis by laser-induced breakdown spectroscopy: A tutorial review, *J. Anal. At. Spectrom.* 34(6), 1047 (2019)
4. J. Ji, W. Song, Z. Hou, L. Li, X. Yu, and Z. Wang, Raw signal improvement using beam shaping plasma modulation for uranium detection in ore using laser-induced breakdown spectroscopy, *Anal. Chim. Acta* 1235, 340551 (2022)
5. D. A. Cremers, Laser-Induced Breakdown Spectroscopy: Theory and Applications, Berlin, Heidelberg: Springer, 2014
6. J. O. Cáceres and J. Y. S. de los Terreros, A real-world approach to identifying animal bones and Lower Pleistocene fossils by laser induced breakdown spectroscopy, *Talanta* 235, 122780 (2021)
7. A. Limbeck, L. Brunnbauer, H. Lohninger, P. Pořízka, P. Modlitbová, J. Kaiser, P. Janovszky, A. Kéri, and G. Galbács, Methodology and applications of elemental mapping by laser-induced breakdown spectroscopy, *Anal. Chim. Acta* 1147, 72 (2021)
8. Z. Hou, M. S. Afgan, S. Sheta, J. Liu, and Z. Wang, Plasma modulation using beam shaping to improve signal quality for laser-induced breakdown spectroscopy, *J. Anal. At. Spectrom.* 35(8), 1671 (2020)
9. K. Amal, S. H. Elnaby, V. Palleschi, A. Salvetti, and M. A. Harith, Comparison between single- and double-pulse LIBS at different air pressures on silicon target, *Appl. Phys. B* 83(4), 651 (2006)
10. C. Gautier, P. Fichet, D. Menut, and J. Dubessy, Applications of the double-pulse laser-induced breakdown spectroscopy (LIBS) in the collinear beam geometry to the elemental analysis of different materials, *Spectrochim. Acta B At. Spectrosc.* 61(2), 210 (2006)
11. Z. Wang, Z. Hou, S. Lui, D. Jiang, J. Liu, and Z. Li, Utilization of moderate cylindrical confinement for precision improvement of laser-induced breakdown spectroscopy signal, *Opt. Express* 20(S6), A1011 (2012)
12. Z. Hou, Z. Wang, J. Liu, W. Ni, and Z. Li, Signal quality

improvement using cylindrical confinement for laser-induced breakdown spectroscopy, *Opt. Express* 21(13), 15974 (2013)
13. R. Yi, X. Yang, F. Lin, and S. Ren, Improving the spectral qualities of major elements in soil by controlling the ambient pressure in time-resolved laser-induced breakdown spectroscopy, *Appl. Opt.* 58(32), 8824 (2019)
14. J. Yu, Z. Hou, Y. Ma, T. Li, Y. Fu, Y. Wang, Z. Li, and Z. Wang, Improvement of laser induced breakdown spectroscopy signal using gas mixture, *Spectrochim. Acta B At. Spectrosc.* 174, 105992 (2020)
15. Y. T. Fu, W. L. Gu, Z. Y. Hou, S. A. Muhammed, T. Q. Li, Y. Wang, and Z. Wang, Mechanism of signal uncertainty generation for laser-induced breakdown spectroscopy, *Front. Phys.* 16(2), 22502 (2021)
16. D. Wu, L. Sun, J. Liu, Y. Lyu, H. Wu, S. Yuan, R. Hai, C. Li, C. Feng, D. Zhao, and H. Ding, Parameter optimization of the spectral emission of laser-induced tungsten plasma for tokamak wall diagnosis at different pressures, *J. Anal. At. Spectrom.* 36(6), 1159 (2021)
17. N. Farid, S. Bashir, and K. Mahmood, Effect of ambient gas conditions on laser-induced copper plasma and surface morphology, *Phys. Scr.* 85(1), 015702 (2012)
18. N. Farid, S. S. Harilal, H. Ding, and A. Hassanein, Emission features and expansion dynamics of nanosecond laser ablation plumes at different ambient pressures, *J. Appl. Phys.* 115(3), 033107 (2014)
19. Z. Haider, Y. B. Munajat, R. Kamarulzaman, and N. Shahami, Comparison of single pulse and double simultaneous pulse laser-induced breakdown spectroscopy, *Anal. Lett.* 48(2), 308 (2015)
20. H. Yuan, A. B. Gojani, I. B. Gornushkin, X. Wang, D. Liu, and M. Rong, Dynamics of laser-induced plasma splitting, *Opt. Lasers Eng.* 124, 105832 (2020)
21. Z. Wang, M. S. Afgan, W. Gu, Y. Song, Y. Wang, Z. Hou, W. Song, and Z. Li, Recent advances in laser-induced breakdown spectroscopy quantification: From fundamental understanding to data processing, *Trends Analyt. Chem.* 143, 116385 (2021)
22. A. J. Effenberger and J. R. Scott, Effect of atmospheric conditions on LIBS spectra, *Sensors* 10, 4907 (2010)
23. M. Burger, D. Pantić, Z. Nikolić, and S. Djeniže, Shielding effects in the laser-generated copper plasma under reduced pressures of He atmosphere, *J. Quant. Spectrosc. Radiat. Transf.* 170, 19 (2016)
24. J. R. Scott, A. J. Effenberger, and J. J. Hatch, Influence of Atmospheric Pressure and Composition on LIBS, in: Laser-Induced Breakdown Spectroscopy: Theory and Applications, Berlin, Heidelberg: Springer, 2014
25. J. S. Cowpe, R. D. Pilkington, J. S. Astin, and A. E. Hill, The effect of ambient pressure on laser-induced silicon plasma temperature, density and morphology, *J. Phys. D* 42(16), 165202 (2009)
26. T. Li, S. Sheta, Z. Hou, J. Dong, and Z. Wang, Impacts of a collection system on laser-induced breakdown spectroscopy signal detection, *Appl. Opt.* 57(21), 6120 (2018)
27. S. Bashir, N. Farid, K. Mahmood, and M. Shahid Rafique, Influence of ambient gas and its pressure on the laser-induced breakdown spectroscopy and the surface morphology of laser-ablated Cd, *Appl. Phys. A* 107(1), 203 (2012)
28. R. Noll, Laser-Induced Breakdown Spectroscopy: Fundamentals and Applications, Berlin, Heidelberg: Springer, 2012